

Article

Theoretical Modeling and Mechanical Characterization at Increasing Temperatures under Compressive Loads of Al Core and Honeycomb Sandwich

Alessandra Ceci, Girolamo Costanza *  and Maria Elisa Tata 

Industrial Engineering Department, University of Rome Tor Vergata, 00133 Rome, Italy; alessandra.ceci@uniroma2.it (A.C.); elisa.tata@uniroma2.it (M.E.T.)

* Correspondence: costanza@ing.uniroma2.it; Tel.: +39-06-72597185

Abstract: This work investigates the mechanical behavior under out-of-plane compression of the Al core and honeycomb sandwich at increasing temperatures of up to 300 °C. After the first introductory theoretical modeling on room-temperature compressive behavior, the experimental results at increasing temperatures up to 300 °C are presented and discussed. The analysis of the results shows that peak stress, plateau stress, and specific absorbed energy gradually decrease as the temperature increases. The final densification occurs always at the same strain level (around 75%). Sandwich honeycomb test temperatures have been limited to 200 °C for bonding problems of the skin to the sandwich due to the glue. The experimental and modeling results agree well at room temperature as well at increasing temperatures. The results can provide useful information to choose base materials for greater energy absorption at increasing temperatures.

Keywords: honeycomb panels; compressive behavior; modeling; mechanical characterization



Citation: Ceci, A.; Costanza, G.; Tata, M.E. Theoretical Modeling and Mechanical Characterization at Increasing Temperatures under Compressive Loads of Al Core and Honeycomb Sandwich. *Metals* **2024**, *14*, 544. <https://doi.org/10.3390/met14050544>

Academic Editor: Afsaneh Rabiei

Received: 14 March 2024

Revised: 21 April 2024

Accepted: 30 April 2024

Published: 3 May 2024



Copyright: © 2024 by the authors. Licensee MDPI, Basel, Switzerland. This article is an open access article distributed under the terms and conditions of the Creative Commons Attribution (CC BY) license (<https://creativecommons.org/licenses/by/4.0/>).

1. Introduction

Honeycomb-based materials are cellular structures that show high versatility for the many engineering features that distinguish them [1]. They combine stiffness and strength, with an extraordinary lightness of the structure as well as excellent absorption capabilities [2,3]. In the last decade, sandwich structures with a honeycomb cellular core have been employed widely as structural elements in aerospace, naval, and high-performance vehicles thanks to the high bending stiffness and reduced weight in comparison with traditional materials. This structure is made up of a central “core” made of a lightweight and cellular assembly and two external sheets called “skins”. Many animals and plant organisms exhibit such a cellular organization; such structured materials have always been part of the natural world. However, it was only in the first half of the twentieth century that mankind began to employ them in large-scale productions through a detailed approach of bio-inspiration [4]. Since then, honeycomb technology has made great strides, and to date, it represents a consolidated industrial reality. Recent works can be found in the literature describing honeycomb panel characterization [5] and sandwiches under different loading conditions (compression [6–8], bending [9,10], and shear [11–13]), but none of them consider the effect of temperature on the mechanical behavior. The main advantages of sandwich structures are high strength and energy absorption in crashes and upon impact [14–17] and thermal and acoustic insulation [18]. Obtaining information about the mechanical properties at increasing temperatures is crucial in many industrial fields, such as aerospace, for example, in order to develop reusable launch vehicles [19]. In this experimental work, only Al honeycomb has been considered; however, different honeycomb materials can be manufactured, such as phenolic resin reinforced with quartz, and glass and carbon fiber for demonstrator parts (antenna reflector; Vespa structure) for applications in space applications [20].

In this study, the main properties and applications of honeycombs are briefly introduced, focusing the attention on biomimicry [21], the process of intelligent imitation of nature [22]. The compression behavior of hexagonal honeycomb and sandwich structures has been analyzed at increasing test temperatures. In the experimental part of this study, mechanical characterization is performed under the compression out of the plane of alveolar samples in Al alloys. The experimental results are presented and discussed with reference to the impact of temperature on the main mechanical properties and to the different behaviors of a simple honeycomb and an alveolar-core sandwich. Compression tests have been performed at the following temperatures: 20 °C, 100 °C, 200 °C, and 300 °C for Al honeycomb and 20 °C, 100 °C, and 200 °C for the Al honeycomb sandwich panel. Although in the literature, many papers have focused their attention on the compressive behavior of both materials at room temperature, from an experimental point of view, only one study has been identified for the investigation of the temperature-dependent out-of-the-plane compressive behavior of metallic honeycombs. The present study helps improve our understanding of the temperature-dependent behavior of Al honeycomb and the Al sandwich panel under static out-of-the-plane compression. The discussion provides useful guidelines for the design of Al honeycomb with increased energy absorption at room temperature and higher.

2. Materials and Methods

2.1. Sample Preparation and Geometrical Characterization

Honeycomb samples have been extracted from a large commercial sandwich panel (Al 3000 series alloy) employing a miter saw with a special alumina cutting disc. Samples with a square cross-section of 85 ± 3 mm side have been obtained. Such sandwich honeycomb panels have a standard thickness of 50 mm, while samples made of the core (without the skins) have a 48 mm thickness due to the absence of the skins. In Figure 1a,b, the sandwich and core panels are shown in top view.

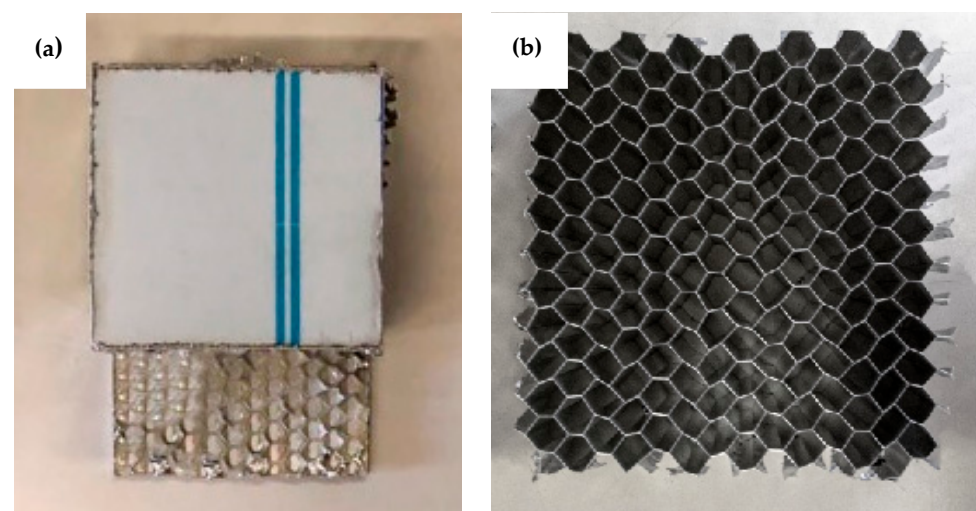


Figure 1. Top view: (a) Al sandwich panel and (b) Al honeycomb core. Reprinted from ref. [6].

The base geometry of the hexagonal honeycomb was analyzed and discussed in detail in an earlier paper [6]. The average wall thickness was 0.05 mm, the common side of the hexagon was 2.9 mm, the bigger side of the hexagon was 4.6 mm, and the angle was 45° , as detailed in Figure 2.

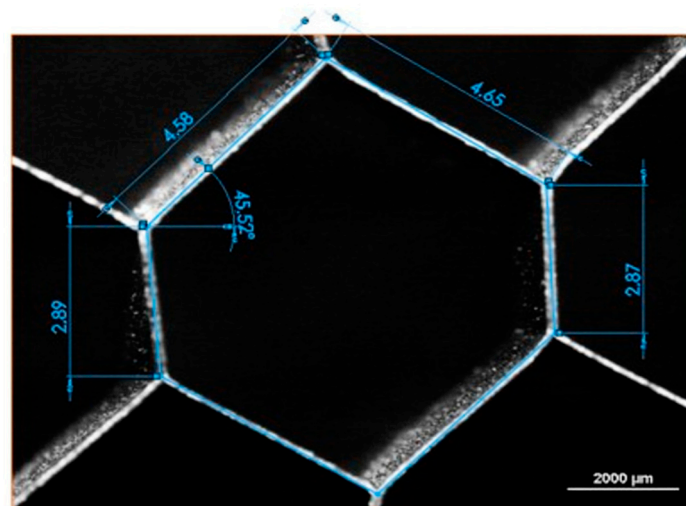


Figure 2. Geometric features of the hexagonal honeycomb cells: $l = 4.6$ mm, $h = 2.9$ mm, and $\alpha = 45^\circ$. Reprinted from ref. [6].

2.2. Experimental Apparatus

Out-of-the-plane compression tests have been performed using an MTS Insight 50 machine (MTS, Eden Prairie, MN, USA) (Figure 3a) in a thermostatic room able to reach temperatures up to 300 °C. The selected configuration is pure normal stress applied with the use of compression plates (Figure 3b) and the adopted temperatures are 20 °C, 100 °C, 200 °C, and 300 °C. The tests are performed according to the ASTM standard C365/365M-22 under quasi-static conditions. The cross-head speed is set at 10 mm/min to complete the whole compression test in 5 min, as required by the standard. The sampling frequency is 5 Hz, and the maximum applied load is 50 kN, which is the machine's maximum capability.

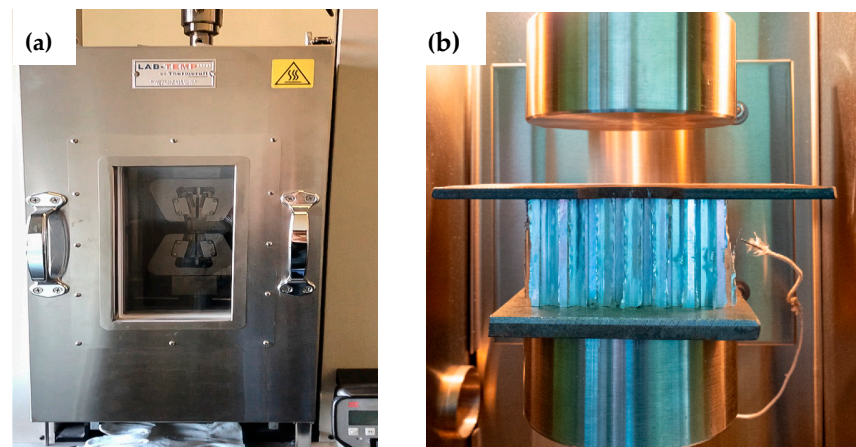


Figure 3. (a) MTS Insight machine in thermostatic room. (b) Compression plates. Reprinted from ref. [6].

3. Theoretical Modeling

Studying the mechanical behavior of a sandwich panel generally starts with a comparison with an I-beam (Figure 4), comparing the skins to the flanges, which take the flexural, compressive, and tensile load alternately, and comparing the honeycomb core to the core of the beam, which support the shear load, separating the skins and increasing the moment of inertia and, consequently, the flexural stiffness. This similarity is completely justified, but it leaves out important aspects that derive from the fact that the adoption of a cellular core makes the material a composite and therefore gives it peculiar characteristics that make it intrinsically different from a simple I-beam.

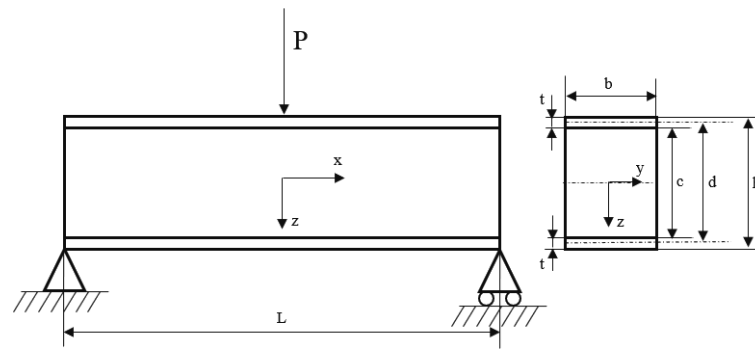


Figure 4. Sandwich beam in bending condition.

The overall flexural stiffness of the sandwich beam, D_s , can be obtained from the Huygens–Steiner theorem and is equal to the sum of the individual contributions given by the different parts that constitute it. It is calculated with respect to the barycentric axis of the overall section (Equation (1)):

$$D^s = E_f \frac{bt^3}{6} + E_f \frac{btd^2}{2} + E^* \frac{bc^3}{12} \tag{1}$$

where E_f is the skin’s elastic modulus, E^* is the core’s elastic modulus, b is the width, t is the thickness, and d is the average height. As usually $E_f \gg E^*$ and $c \cong d \gg t$ the following can be assumed:

$$D^s = E_f \frac{btd^2}{2} \tag{2}$$

Assuming that sections stay plane and parallel to the barycentric axis during deformation, it is possible to calculate the normal tension (s_f) according to the beam theory through the relationship (3) for the skin and (4) for the core as a function of the bending moment (M_z):

$$\sigma_f = E_f \frac{M_z}{D^s} \tag{3}$$

$$\sigma^* = E^* \frac{M_z}{D^s} \tag{4}$$

As $E_f \gg E^*$, $s_f \gg s^*$, and thus the skins almost completely withstand bending stresses.

Regarding the tangential shear stresses, they exhibit a parabolic trend along the entire section. But if the core is weak, as often happens, its contribution to the bending stiffness is negligible, and if the stiffness of the skins is small with respect to their barycentric axes, it is possible to approximate the variation in the shear stress (t) along the skins as linear and constant along the core with the following value:

$$\tau^* = \frac{T}{bd} \tag{5}$$

where T is the shear force on the examined section. The analogies between sandwich beams and I-beams are evident.

3.1. Out-of-the Plane Compression Behavior of Hexagonal Metallic Core

The compression behavior of metallic honeycombs is strongly determined by the geometry of the cell [Figure 5], by the properties of the constituent material of the cell wall, and, in particular, by the relative density, expressible as the following relationship (6):

$$\frac{\rho^*}{\rho^s} = \frac{\left(\frac{t}{l}\right) \left(\frac{h}{l} + 1\right)}{\cos\theta \left(\frac{h}{l} + \sin\theta\right)} \tag{6}$$

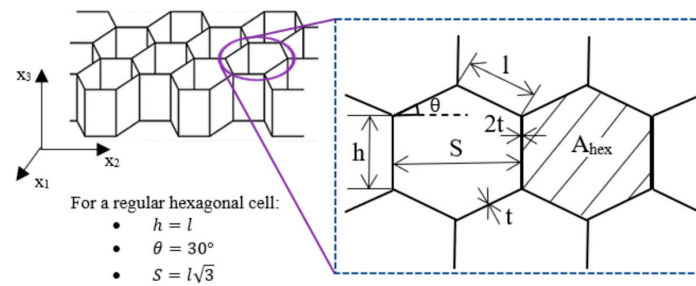


Figure 5. Elementary cell geometry.

Under the hypothesis of small t/l values (and consequently $\frac{\rho^*}{\rho^s}$), and considering that the double-wall thickness due to the production method for hexagonal cells is valid, one can obtain the following (7):

$$\frac{\rho^*}{\rho^s} = \frac{8}{3\sqrt{3}} \frac{t}{l} = \frac{8}{3} \frac{t}{S} \tag{7}$$

The cellular structure makes the honeycombs, and consequently the sandwich panels, intrinsically anisotropic and, in detail, orthotropic, that is, three planes of elastic symmetry orthogonal to each other. It can therefore be considered that the reference system whose axes are parallel to the lines generated by their intersection of such planes has nine independent elastic constants.

The out-of-the-plane compression is considered when the honeycomb core undertakes a monoaxial compression strength in the direction x_3 (Figure 5). If subjected to this kind of load, the honeycomb appears more rigid. The elastic modulus is that of the cell wall divided by the relative density [22] (Equation (8)).

$$E_3^* = E_s \frac{\rho^*}{\rho^s} \tag{8}$$

A typical s^*-e^* curve is shown in Figure 6.

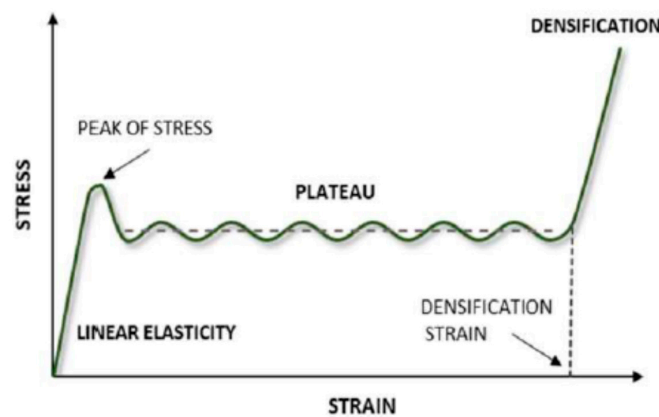


Figure 6. The s^*-e^* curve for an out-of-the-plane compression test of metal honeycomb, reprinted from [15].

The initial trend of the curve is quasi-linear because after reaching the elastic limit of stability, a region is reached in which bending stresses reduce the stiffness of the wall up to the peak stress [16]. The mathematical model proposed here overestimates this limit; so, in the proposed model, the instability load is considered with a reasonable theoretical approximation of $\sigma_{pk,3}^*$ [23]. The critical instability load (P) acting on a single wall (side “ l ”) can be derived by using the classical theory of Timoshenko [24] for the instability of thin sheets homogeneously compressed along a direction:

$$P = \frac{KD}{l^2} \quad (9)$$

where D is the bending stiffness and K depends on the boundary conditions and is related to the constraint imposed by the neighboring cells, the height ratio, and the side of the wall. Detailing for the system under consideration (Zhang [25]):

$$P = \frac{KE_S}{(1 - \nu_S^2)} \frac{t^3}{l} \quad (10)$$

with $K = 5.73$. The peak stress is as follows:

$$\sigma_{pk,3}^* = \frac{10P}{A_{ex}} = \frac{28.65E_S}{(1 - \nu_S^2)\cos\theta(1 + \sin\theta)} \left(\frac{t}{l}\right)^3 \quad (11)$$

Equation (11) has been shown to have low accuracy, especially for honeycombs that are too dense. Better precision has been found with the relationship suggested by Geng [23], with an energetic approach applied to a “Y” cell. For hexagonal regular cells, the following can be found:

$$\sigma_{pk,3}^* = \frac{50E_S}{81\pi} \left(\frac{t}{l}\right)^2 \quad (12)$$

After $\sigma_{pk,3}^*$, the stress falls down to a local minimum due to the onset of the first instability folds in the plastic regime. After that, there is a huge plateau in which various stress oscillations are evident, characteristic of successive instability folds on the cellular walls. At the same time, it is possible to observe a partial detachment of the adhesive bonding between the walls, especially at elevated temperatures.

The calculation of the average plateau stress is ascribable to Wierzbicki [26]:

$$\sigma_{m,3}^* = 6.629\sigma_{y,s} \left(\frac{t}{l}\right)^{5/3} = 16.56\sigma_{y,s} \left(\frac{t}{S}\right)^{5/3} \quad (13)$$

More recently, Geng, et al. [25] have determined new expressions for $\sigma_{m,3}^*$ thanks to the simplified super folding element theory [27]:

$$\sigma_{m,3}^* = \frac{\pi\sigma_{y,s}t^2l + 2\pi\sigma_{y,s}t^2h}{k\sqrt{\pi}tl + 2\pi th\cos\theta(h + l\sin\theta)l} \quad (14)$$

For regular hexagonal cells and $\theta = 30^\circ$,

$$\sigma_{m,3}^* = 7.059\sigma_{y,s} \left(\frac{t}{S}\right)^{\frac{3}{2}} \quad (15)$$

After that, in the final part of the stress–strain curve, a steep stress increase is due to the densification process in which the cell walls collapse on themselves.

3.2. Energy Absorption

The area under the s-e curve is equivalent to the energy absorbed in units of volume (U):

$$U = \int_0^\varepsilon \sigma(\varepsilon)d\varepsilon \quad (16)$$

From a practical point of view, the absorbed energy is more interesting before the final densification stage of the curve, which is up to ε_d^* . This is because due to the fast increase in the stress, the energy absorption falls down dramatically.

$$U = \int_0^{\varepsilon_d^*} \sigma^* \varepsilon^* d\varepsilon^* \quad (17)$$

A useful indicator for the evaluation of the resistance performance in crashes is the specific energy absorption (SEA), defined as follows:

$$SEA = \frac{V^* U^*}{m^*} = \frac{V^* \int_d^{\varepsilon_d^*} \sigma^*(\varepsilon^*) d\varepsilon^*}{m^*} = \frac{\int_d^{\varepsilon_d^*} \sigma^*(\varepsilon^*) d\varepsilon^*}{\rho^*} \quad (18)$$

From the information of the $\sigma^* - \varepsilon^*$ curve, it is possible to obtain the average plateau stress:

$$\sigma_m^* = \frac{\int_{\varepsilon_{pk}^*}^{\varepsilon_d^*} \sigma^*(\varepsilon^*) d\varepsilon^*}{\varepsilon_d^* - \varepsilon_{pk}^*} \quad (19)$$

Assuming $\varepsilon_{pk}^* = 0$, it is possible to estimate the SEA:

$$SEA = \frac{V^* U^*}{m^*} = \frac{\sigma_m^* \varepsilon_d^*}{\rho^*} \quad (20)$$

For the effect of temperature on Al honeycomb, values of peak stress, plateau stress, and specific energy absorption (SEA) have been found in the literature at increasing test temperatures [28]. All of them have been evaluated with the energy method proposed by Wierzbicki et al. [26,29,30], in which theoretical and modeling results show good agreement in terms of trends and absolute values.

4. Experimental Results and Discussion

The compression tests have been performed in the out-of-plane loading condition. Three repetitions have been performed for each type of sample to assess the repeatability of the results. The stress–strain curves reported in the following graphs were calculated considering the vertical force measured by the load cell divided by the whole surface of the sample, while for the strain, the measurement displacement of the crosshead was divided by the initial height of each sample and reported as a percentage (%). The “toe region” in the first part of the stress–strain curve, which did not reflect the properties of the real material and is ascribable to the misalignment of the test sample, was compensated for, and after this correction, the right position on the X axis was achieved. The pictures collected in successive steps (20% each step) during the compression tests at 20 °C are reported in Figure 7.



Figure 7. Sequence of pictures collected during compression tests at room temperature (20% each) for core (left) and honeycomb sandwich (right).

4.1. Al Core Compression Tests

Compression tests on the Al core have been performed at 20 °C, 100 °C, 200 °C, and 300 °C, with samples thermostated for 20 min at the test temperature before starting the compression tests. The results are illustrated in Figure 8.

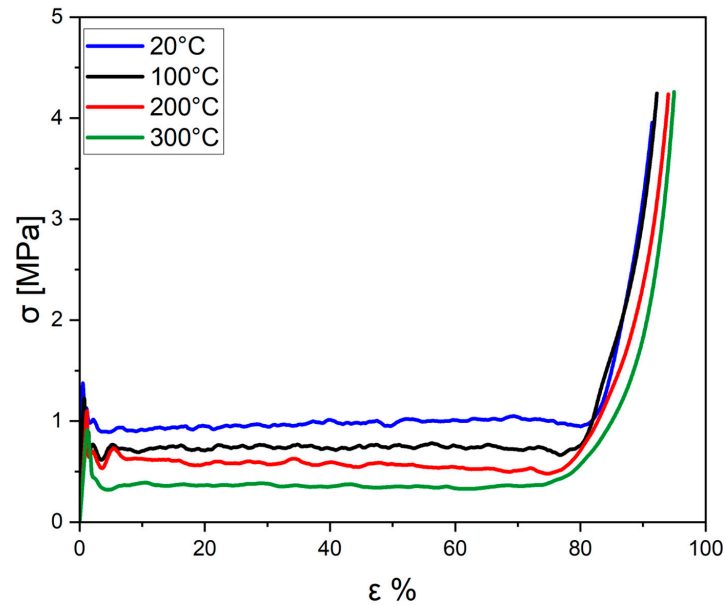


Figure 8. Compression test curves (comparison) for Al core compressed at 20 °C, 100 °C, 200 °C, and 300 °C.

In each compression curve, there is always a linear stage of the stress–strain trend followed by a peak stress, ascribable to the formation of the first instability lobe (the first folding of the cell wall). The peak is immediately followed by a fall in the stress and a successive wide region in which the stress is nearly constant (plateau). The plateau extends up to 80% of the strain, with small fluctuations due to the formation of successive folds, and is finally followed by a steep increase in the load when there is no more possibility of cell deformation and the final densification occurs. From the comparison of the curves, the following trends are evident:

- (1) The peak stress reduces as the temperature increases;
- (2) The plateau stress reduces as the temperature increases;
- (3) The specific absorbed energy (the area below the curve) decreases as the temperature increases;
- (4) The final densification occurs always at the same strain level (around 80%).

The detailed courses of the curves up to 10% strain are highlighted in Figure 9, and the experimental results are displayed in Table 1.

Table 1. Experimental results for Al core compression tests.

Test Temperature (°C)	σ_{pk}^* (MPa)	σ_m^* (MPa)	ϵ_d^* (%)	U^* (J/cm ³)
20	1.4	1.0	80	0.8
100	1.2	0.7	77	0.6
200	1.1	0.6	75	0.4
300	0.9	0.4	73	0.2

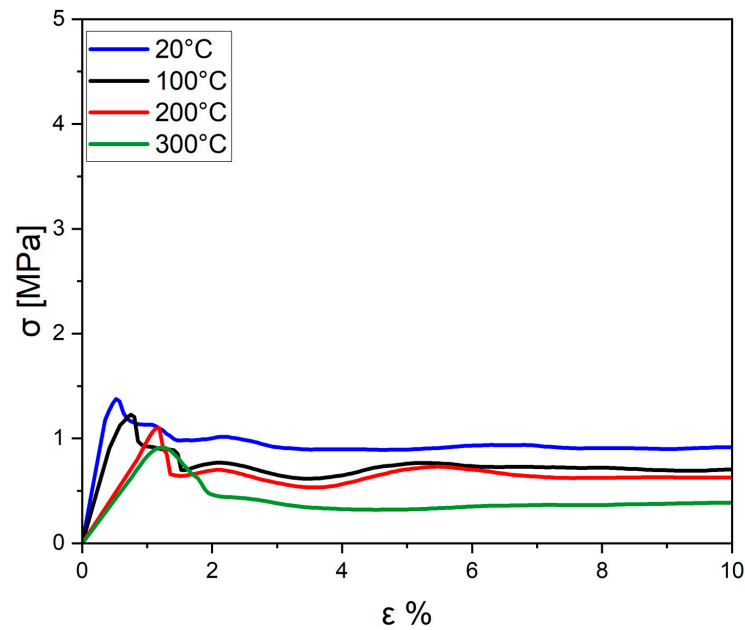


Figure 9. Compression stress–strain curves up to 10% strain for Al core at increasing test temperatures.

The modeling results, at room temperature as well up to 300 °C, are reported in Table 2 according to [28].

Table 2. Modeling results for Al core compression tests.

Test Temperature (°C)	σ_{pk}^* (MPa)	σ_m^* (MPa)	ε_d^* (%)	U^* (J/cm ³)
20	2.7	0.41	n.a.	0.4
100	2.2	0.33	n.a.	0.3
200	1.8	0.27	n.a.	0.25
300	1.3	0.21	n.a.	0.20

As evidenced in the comparison between Tables 1 and 2, all of the considered properties (peak stress, plateau stress, and specific absorbed energy) exhibit the same decreasing trend when the temperature increases, both in the experimental and modeling results.

4.2. Honeycomb Sandwich Compression Tests

The honeycomb sandwich compression tests have been performed at 20 °C, 100 °C, and 200 °C, with samples maintained for 20 min at the test temperature before compression. Comparative results are shown in Figure 10, and all experimental results are summarized in Table 3. The tests on the honeycomb sandwich have not been performed at 300 °C due to the reduced performance of the glue used for the anchoring of the skins to the honeycomb. The detailed courses of the curves up to 10% strain are highlighted in Figure 11.

Table 3. Experimental results for honeycomb sandwich compression tests.

Test Temperature (°C)	σ_{pk}^* (MPa)	σ_m^* (MPa)	ε_d^* (%)	U^* (J/cm ³)
20	2.0	1.1	67	0.65
100	1.4	0.7	66	0.47
200	1.0	0.5	64	0.36

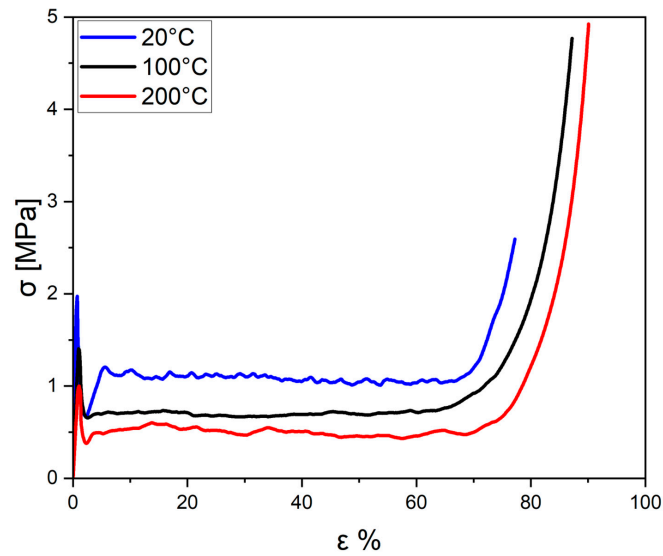


Figure 10. Compression test curves (comparison) for honeycomb sandwich compressed at 20 °C, 100 °C, and 200 °C.

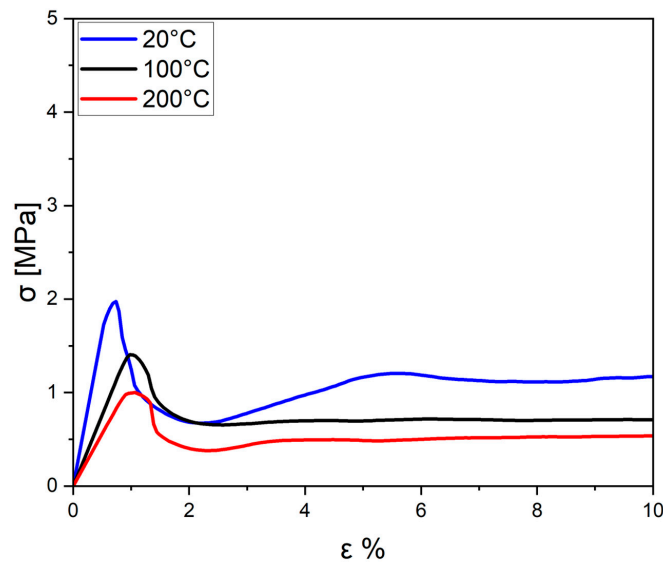


Figure 11. Comparison of compression stress–strain curves up to 10% strain for honeycomb sandwich at increasing test temperatures.

In each compression curve, there is always a linear stage of the stress–strain trend followed by a peak stress, ascribable to the formation of the first instability lobe (the first folding of the cell wall of the core inside the sandwich). The peak is immediately followed by a fall in the stress and a successive wide region in which the stress is nearly constant (plateau). The plateau extends up to 70% of the strain, with small fluctuations due to the formation of successive folds, and finally, it is followed by a steep increase in the load when there is no longer any possibility of cell deformation and the final densification occurs. From the comparison of the curves, the following trends are evident:

- (1) The peak stress reduces as the temperature increases;
- (2) The plateau stress reduces as the temperature increases;
- (3) The specific absorbed energy (the area below the curve) decreases as the temperature increases;
- (4) The final densification occurs always at the same strain level (around 75%);

- (5) At increasing temperatures, a higher strain of the sandwich can be achieved mainly due to the softening in the behavior of the Al core. This phenomenon is more evident for the honeycomb sandwich compared to the pure Al core.

The experimental results and trends illustrated in this article are aligned with the modeling results presented by Whang et al. in a recent study [28]. These results can provide useful information about the change in the mechanical properties of the Al core and the honeycomb sandwich at increasing temperatures.

No modeling results have been found in the literature for Al honeycomb. As a consequence of that, it has not been possible to make comparisons between the experimental and modeling results at increasing temperatures for the honeycomb sandwich.

5. Conclusions and Future Work

In this work, the experimental results of compression tests conducted at increasing test temperatures (from 20 °C to 300 °C) for the Al core and honeycomb sandwich under out-of-the-plane loading conditions are presented and discussed. The effect of temperature on the mechanical properties and specific energy absorption has been analyzed from an experimental and theoretical point of view for the two materials considered. The main conclusions are given in the following:

1. The peak stress, the plateau stress, and the specific energy absorption gradually decrease as the test temperature increases;
2. The densification strain moderately decreases with increasing test temperature;
3. The final densification occurs always at the same strain level: around 75% for the Al core and around 65% for the honeycomb sandwich;
4. At increasing temperatures, a higher strain of the sandwich can be achieved mainly as a result of the softening in the behavior of the Al core. This phenomenon is more evident for the honeycomb sandwich than for the pure Al core;
5. The aluminum honeycomb sandwich cannot be used at temperatures higher than 200 °C due to the presence of the glue between the core and the panel.

The aluminum honeycomb sandwich can be very useful in fields where crash energy absorption and lightness are fundamental, such as in the automotive and railway application fields.

Author Contributions: Conceptualization, G.C. and M.E.T.; methodology, A.C., G.C. and M.E.T.; software, A.C., G.C. and M.E.T.; validation, A.C., G.C. and M.E.T.; formal analysis, A.C., G.C. and M.E.T.; investigation, A.C., G.C. and M.E.T.; resources, A.C., G.C. and M.E.T.; data curation, A.C.; writing—original draft preparation, A.C., G.C. and M.E.T.; writing—review and editing, A.C., G.C. and M.E.T.; visualization, A.C., G.C. and M.E.T.; supervision, G.C. and M.E.T.; project administration, A.C., G.C. and M.E.T.; funding acquisition, G.C. and M.E.T. All authors have read and agreed to the published version of the manuscript.

Funding: This research received no external funding.

Data Availability Statement: The raw data supporting the conclusions of this article will be made available by the authors on request.

Acknowledgments: The authors are grateful to Piero Plini and Benedetto Iacovone for their technical assistance in sample preparation and the experimental procedures.

Conflicts of Interest: The authors declare no conflicts of interest.

References

1. Du Plessis, A.; Razavi, N.; Benedetti, M.; Murchio, S.; Leary, M.; Watson, M.; Bhate, D.; Berto, F. Properties and applications of additively manufactured metallic cellular materials. *Prog. Mat. Sci.* **2022**, *125*, 100918. [[CrossRef](#)]
2. Banhart, J. Manufacture, characterization and application of cellular metals and metal foams. *Prog. Mat. Sci.* **2001**, *46*, 559–632. [[CrossRef](#)]
3. Costanza, G.; Tata, M.E. Mechanical behavior of PCMT and SDP al foams: A review. *Proc. Struct. Int.* **2020**, *25*, 161742. [[CrossRef](#)]

4. Zhang, Q.; Yang, X.; Li, P.; Huang, G.; Feng, S.; Shen, C.; Han, B.; Zhang, X.; Jin, F.; Xu, F.; et al. Bioinspired engineering of honeycomb structure- Using nature to inspire human innovation. *Prog. Mat. Sci.* **2015**, *74*, 332–400. [[CrossRef](#)]
5. Costanza, G.; Ferrigno, S.; Tata, M.E. Static compression study of honeycomb panel. *Met. It.* **2021**, *113*, 13–21.
6. Arquilla, G.; Ceci, A.; Costanza, G.; Tata, M.E. Effect of the load application angle on the compressive behavior of Al honeycomb under combined normal-shear stress. *Materials* **2023**, *16*, 5462. [[CrossRef](#)] [[PubMed](#)]
7. Yu, X.; Zhou, J.; Liang, H.; Jiang, Z.; Wu, L. Mechanical metamaterials associated with stiffness, rigidity and compressibility: A brief review. *Prog. Mat. Sci.* **2018**, *94*, 114–173. [[CrossRef](#)]
8. Ge, L.; Zheng, H.; Li, H.; Lu, B.; Su, H.; Fang, D. Compression behavior of a novel sandwich structure with bi-directional corrugated core. *Thin-Wall. Struct.* **2021**, *161*, 107413. [[CrossRef](#)]
9. Mani, M.; Thiyagu, M.; Krishnan, P.K. Flexural and compression behavior analysis of hybrid sandwich composites with nano silicon particles in low-velocity impact analysis. *Mater. Today Proc.* **2023**. [[CrossRef](#)]
10. Xia, M.; Takayanagi, H.; Kemmochi, K. Bending behavior of filament-wound fiber-reinforced sandwich pipes. *Compos. Struct.* **2002**, *56*, 201–210. [[CrossRef](#)]
11. Mostafa, A.; Shankar, K.; Morozov, E.V. Insight into the shear behavior of composite sandwich panels with foam core. *Mater. Des.* **2013**, *50*, 92–101. [[CrossRef](#)]
12. Manalo, A.; Aravinthan, T.; Karunasena, W. Shear behavior of glue-laminated composite sandwich beams. In *Advances in FRP Composites in Civil Engineering: Proceedings of the 5th International Conference on FRP Composites in Civil Engineering (CICE 2010), Beijing, China, 27–29 September 2010*; Springer: Berlin, Germany, 2011. [[CrossRef](#)]
13. Cong, L.; Sun, Y. Study on transverse shear behavior of CFRP sandwich structure with M-pattern folded core. *Appl. Mech. Mater.* **2014**, *670–671*, 173–176. [[CrossRef](#)]
14. Han, T.S.; Ural, A.; Chen, C.S.; Zehnder, A.T.; Ingraffea, A.R.; Billington, S.L. Delamination buckling and propagation analysis of honeycomb panels using a cohesive element approach. *Int. J. Fract.* **2002**, *115*, 101–123. [[CrossRef](#)]
15. Stanzack, M.; Fras, T.; Blanc, L.; Pawlowski, P.; Rusinek, A. Blast-induced compression of a thin-walled aluminum honeycomb structure-experiment and modeling. *Metals* **2019**, *9*, 1350. [[CrossRef](#)]
16. Wilbert, A.; Yang, W.Y.; Kyriakides, S.; Flocari, J.F. Buckling and progressive crushing of laterally loaded honeycomb. *Int. J. Sol. Struct.* **2011**, *48*, 803–816. [[CrossRef](#)]
17. Quoc, P.M.; Krzikall, D.; Mesicek, J.; Petru, J.; Smirau, J.; Sliva, A.; Poruba, Z. On Aluminum Honeycomb Impact Attenuator Designs for Formula Student Competitions. *Symmetry* **2020**, *12*, 1647. [[CrossRef](#)]
18. Shi, G.; Wu, X.; Jiang, R.; Li, S. A particle reinforced gradient honeycomb sandwich panel for broadband insulation. *Mathematics* **2023**, *11*, 502. [[CrossRef](#)]
19. Wu, W.; Xia, R.; Qian, G.; Liu, Z.; Razavi, N.; Berto, F.; Gao, H. Mechanostructures; rational mechanical design, fabrication, performance evaluation and industrial application of advanced structures. *Prog. Mat. Sci.* **2023**, *131*, 101021. [[CrossRef](#)]
20. Putz, M.; Lafont, U.; Wittlich, M.; Markestein, E.; Herrmann, C.; Fischer, H. 3D Honeycomb for advanced manufacturing for space application. *CEAS Space J.* **2023**, *15*, 203–211. [[CrossRef](#)]
21. Schmitt, O. Some interesting and useful biomimetic transforms. In *Proceeding, Third International Biophysics Congress, Boston, MA, USA, 29 August–3 September 1969*; National Institutes of Health (NIH): Boston, MA, USA, 1969.
22. Hwang, J.; Jeong, Y.; Park, J.M.; Lee, K.H.; Hong, J.W.; Choi, J. Biomimetics: Forecasting the future of science, engineering and medicine. *Int. J. Nanomed.* **2015**, *10*, 5701–5713. [[CrossRef](#)]
23. Geng, X.; Liu, Y.; Zheng, W.; Wang, Y.; Li, M. Prediction of crushing response for metal hexagonal honeycomb under quasi-static loading. *Shock Vib.* **2018**, *2018*, 8043410. [[CrossRef](#)]
24. Timoshenko, S.P.; Gere, J. *Theory of Elastic Stability*; Dover Publications: New York, NY, USA, 1961.
25. Zhang, J.; Ashby, M.F. The out-of-the-plane properties of honeycombs. *Int. J. Mech. Sci.* **1992**, *34*, 475–489. [[CrossRef](#)]
26. Wierzbicki, T.; Abramowicz, W. On the crushing mechanics of thin-walled structures. *J. Appl. Mech.* **1983**, *50*, 727–734. [[CrossRef](#)]
27. Chen, W.; Wierzbicki, T. Relative merits of single-cell, multi-cell and foam-filled thin walled structures in energy absorption. *Thin-Wall. Struct.* **2001**, *39*, 287–306. [[CrossRef](#)]
28. Wang, S.; Li, W.; Tao, Y.; Zhang, X.; Zhang, X.; Li, Y.; Deng, Y.; Shen, Z.; Zhang, X.; Xu, J.; et al. Investigation on the temperature dependent out-of-plane quasi-static compressive behavior of metallic honeycombs. *Thin-Wall. Struct.* **2020**, *149*, 106625. [[CrossRef](#)]
29. Wierzbicki, T. Crushing analysis of metal honeycombs. *Int. J. Imp. Eng.* **1983**, *1*, 157–174. [[CrossRef](#)]
30. Abramowicz, W.; Wierzbicki, T. Axial crushing of multicorner sheet metal columns. *J. Appl. Mech.* **1989**, *56*, 113–120. [[CrossRef](#)]

Disclaimer/Publisher’s Note: The statements, opinions and data contained in all publications are solely those of the individual author(s) and contributor(s) and not of MDPI and/or the editor(s). MDPI and/or the editor(s) disclaim responsibility for any injury to person or property resulting from any ideas, methods, instructions or products referred to in the content.